Draft version September 13, 2018
Typeset using LaTeX **twocolumn** style in AASTeX62

Is Active Galactic Nuclei Feedback Necessary to Get Galaxy Sizes Right?

Tyler Parsotan,[1] Christopher Hayward,[2] Daniel Angles-Alcazar,[2] Jennifer Lotz,[3] and Rachel Cochrane[4,5]

[1]*Department of Physics, Oregon State University, 301 Weniger Hall, Corvallis, OR 97331, U.S.A.*
[2]*Center for Computational Astrophysics, Flatiron Institute, 162 Fifth Avenue, New York, NY 10010, USA*
[3]*Space Telescope Science Institute, 3700 San Martin Dr., Baltimore, MD 21218, USA*
[4]*SUPA, Institute for Astronomy, Royal Observatory Edinburgh, EH9 3HJ, UK*
[5]*Isaac Newton Group of Telescopes, E-38700 Santa Cruz de La Palma, Canary Islands, Spain*

ABSTRACT

Mock observations of simulated galaxies play an important role in ensuring that simulations are able to recover characteristics of observed galaxies. One important property that can be used to facilitate comparisons between simulated and observed galaxies is the stellar mass surface density. We use the SKIRT radiative transfer code to conduct mock observations of the FIRE-2 galaxies at z=1, which have no Black Hole feedback, and observationally recover the stellar mass surface densities within the inner 1 kpc (Σ_1) and half-light radius (Σ_e). When we compare the mock observations to the scaling relations for $\Sigma_1 - M_\star$ and $\Sigma_e - M_\star$ we find that some of the halos are able to recover the $\Sigma_1 - M_\star$ relation. Three out of four halos are over dense with respect to the observationally expected Σ_e, while one halo, which merged with another galaxy recently in its' history, has a Σ_e that is in agreement with observations. We additionally produce mock images of the FIRE-2 galaxies at rest frame 0.5 μm which are fitted with a Sersic profile to find half light radii of the mock observations, R_e. We find that the acquired R_e are smaller than what is observationally expected by the size-mass relationship. The combination of some of the galaxies lying on the $\Sigma_1 - M_\star$ relation and having small R_e suggests that the halos need to have more stars further from the central region of the galaxy, while maintaining the central density.

1. INTRODUCTION

Active Galactic Nuclei (AGN) are supermassive black holes (BHs) at the center of massive galaxies that are accreting material and emitting the released energy across the electromagnetic spectrum. In general, AGN are expected to have an affect on the galaxy which hosts them. This idea is supported by a variety of observations such as the existence of the observed $M_{\rm BH}-\sigma$ relation, the relationship between the BH mass and the velocity dispersion of the stars within the galaxy (Gültekin et al. 2009). Despite the mounting observational evidence that AGN do affect galaxies, the exact manner in which AGN feedback plays a role in galaxy formation is still not well understood.

One cause for this lack of understanding originates from the Feedback In Realistic Environments (FIRE) cosmological "zoom-in" simulations (Hopkins et al. 2014a) being able to reproduce the observed qualities of galaxies without implementing the physics of AGN feedback (see e.g. Hopkins et al. (2014b); Ma et al. (2015); El-Badry et al. (2016); Feldmann et al. (2017); Anglés-Alcázar et al. (2017a) and many others). These simulations include a variety of stellar feedback physics and are able to resolve and explicitly treat the multiphase interstellar medium of the simulated galaxies.

Recently, the FIRE code has been updated and additional physics have been added to make simulating stellar feedback more realistic (Hopkins et al. 2018); this updated code is known as the FIRE-2 code. Anglés-Alcázar et al. (2017b) used the FIRE-2 code to resimulate a suite of halos from Feldmann et al. (2017), while adding a larger density threshold for star formation, better resolution, and the treatment of BH accretion as being proportional to torques on the accretion disc (Hopkins & Quataert 2011). These improvements over the original MassiveFIRE halos allowed Anglés-Alcázar et al. (2017b) to investigate how the BHs in massive galaxies evolve over time in relation to the observed $M_{\rm BH} - M_{\rm bulge}$ relation.

In the simulations analyzed by Anglés-Alcázar et al. (2017b) the masses of the BHs are appropriate for AGN activity, however, there is no BH feedback implemented. As a result, we would expect that the cores of these galaxies would be too dense compared to what is observationally expected by the $\Sigma_1 - M_\star$ and $\Sigma_e - M_\star$ relations (Barro et al. 2017). Additionally, the Sersic fitted half light radii of these simulated galaxies should

also differ from the $R_e - M_\star$ of observed galaxies (Sersic 1968; van der Wel et al. 2014).

Spatial resolution, projection effects, dust gradients, and other effects (e.g. see Wuyts et al. (2010)), make it challenging to infer properties of a galaxy from an observed 2D surface brightness. Observers attempt to infer a galaxy's properties by fitting models to the galaxy; however, if the inferred properties of the galaxy are in strain with properties of simulated galaxies, it becomes unclear if the simulations or fitted models are incorrect (or both).

This issue can be avoided by modelling observables from simulations, where we know the ground truth. Thus, we can directly compare the results of simulations to observationally acquired properties of galaxies and also test the accuracy of the observational methods used to analyze galaxies.

Here, we have performed post processing radiative transfer on the four halos presented in Anglés-Alcázar et al. (2017b) to generate broadband images that are convolved with a typical point spread function to mimic the effects of finite resolution. We then analyze the simulated images in the same manner as observational data. [1] We fit the images with Sersic profiles, to minimize the effects of the point spread function, and derive properties such as the half light radius, the mass to light ratio, and the stellar mass surface density. We use these quantities to make comparisons with the scaling relations presented by van der Wel et al. (2014) and Barro et al. (2017).

In section 2 of this paper is we outline how the mock images are created and how we measure the stellar mass surface densities and the half light radius of each halo. In section 3 we present the results of the analysis and in section 4 we summarize the comparisons that have been made and discuss the implications in the framework of AGN feedback.

2. METHODS

The four halos from the A series of MassiveFIRE galaxies presented in Anglés-Alcázar et al. (2017b), are the same ones used in this paper. These halos are evolved to z=1 (Anglés-Alcázar et al. 2017b) where we conduct the analysis described here. The simulations use the N-body+hydrodynamics code GIZMO (Hopkins 2015), a more accurate BH accretion model (Anglés-Alcázar et al. 2017b) and the updated FIRE-2 code, to simulate stellar feedback with a higher degree of accuracy (Hopkins et al. 2018) .

We use the SKIRT Monte Carlo radiative transfer code (Camps & Baes 2015) to simulate the effects of the stellar light and the dust in the FIRE-2 galaxies. The code launches photons from star particles and self consistently scatters and absorbs the photons where appropriate. SKIRT allows us to place detectors at 5 different angles around the galaxy to create mock observations at different inclinations. This allows us to incorporate uncertainties that may arise due to viewing effects into our analysis. We use SKIRT with a dust to gas ratio of 0.4, the Starburst99 model for the stellar SEDs (Leitherer et al. 1999) and the Milky Way dust model from Weingartner & Draine (2001). This is the same setup used by Cochran et. al. (in prep).

The SKIRT outputs are then used to construct bandpass images that include the effects of the given bandpass' transmission function, which are acquired from the SVO Filter Profile Service. We construct Johnson B and Kron-Cousins R bandpass images for each inclination angle. The bandpass images are then convolved with a Hubble Space Telescope point spread function (PSF) with a full width half maximum (FWHM) of 0.16" which is a relatively conservative value of the PSF's FWHM (Skelton et al. 2014). For simplicity, we use this PSF for all bandpass images.

Once we have the convolved images in the bandpasses that we are interested in, we use the Statmorph python code (Rodriguez-Gomez 2018) to fit the B-band image of the galaxy with a Sersic profile (Sersic 1968); statmorph attempts to account for the PSF in order to fit the intrinsic light distribution of the galaxy. Using the Sersic profile ellipticity, angle of rotation, and R_e, the half-light radius, we produce an image of the fitted 2D Sersic profile. Then, we calculate the light surface brightness densities, of the fitted Sersic profile, within elliptical apertures with semimajor axis that correspond to 1 kpc and R_e. These light surface brightness densities, σ_B, are calculated as

$$\sigma_b = \frac{\sum_{i,j<1\mathrm{kpc}} I_{ij}}{A} \quad (1)$$

where I_{ij}, in units of $\mathrm{Wm^{-2}arcsec^{-2}}$, is the surface brightness of each pixel that lies within the elliptical aperture and A is the area of the elliptical aperture in square pixels.

Since we wish to infer stellar mass surface densities from the synthetic images in the same manner as observers, we attempt to infer the mass-to-light ratio based on the simulated galaxies' colors (rather than using the true value). In order to calculate the mass to light ratio in the B-band, M/L_B, we follow the method outlined

[1] For simplicity we do not consider uncertainties in recovering the total stellar mass, $M_\star$. In principle biases in recovering $M_\star$ would affect our comparisons with observations, however, various works have found that $M_\star$ can be recovered within ~ 0.3 dex.

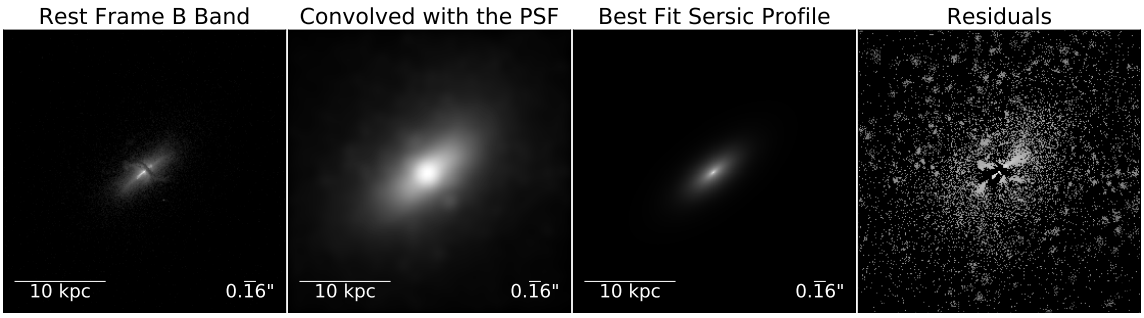

Figure 1. The B bandpass image produced from the SKIRT radiative transfer calculation is shown on the far left panel. In the next panel is the B band image convolved with the PSF. The next panel shows the statmorph fitted Sersic 2D profile that is able to reproduce the SKIRT produced image on the left panel. The last panel shows the residuals, on a log scale, of the best fit Sersic 2D profile subtracted from the "original" unconvolved SKIRT B band image. Typically, the Sersic profile fits are able to account for $\gtrsim$90% of the light in the "original" SKIRT image. The scale bars show 10 kpc, and the FWHM, 0.16", of the PSF that is used in the convolution.

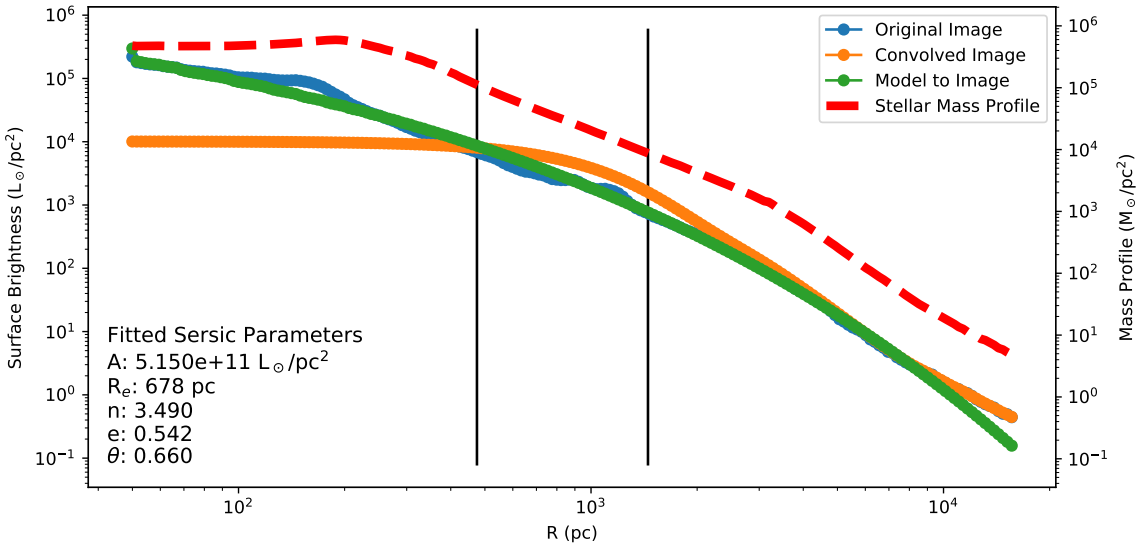

Figure 2. Calculating the surface brightness profiles of the "original" unconvolved SKIRT image and the best fit 2D Sersic profiles (as shown in Figure 1) show that the Sersic profile is able to reconstruct the unconvolved image, as is shown by the blue and the green lines respectively. The fitted Sersic parameters from the statmorph fit are provided on the plot. The convolved image, shown by the orange line, shows the effect of the PSF smearing out the light in the inner 1 kpc of the galaxy. The mass profile of the projected stellar mass map is shown by the red dotted lines. Additionally, the two vertical lines show the statmorph fitted R_{20} and R_{80}, on the left and right respectively.

in Bell & de Jong (2001). We calculate the B-R color magnitude, using the aforementioned bandpass images, and use the fitted relationship given by their Table 4. This relationship is:

$$\log_{10}(M/L_{\rm B}) = 1.03(B-R) - 0.88 \qquad (2)$$

which is Bell & de Jong's (2001) Bruzal and Charlot Scaled Salpeter IMF model for the B-R color. We use their fit for a metallicity of 0.02, however, they showed that the metallicity does not greatly affect $M/L_{\rm B}$ (see their Figure 2(a)).

In order to acquire the B-R color, we follow Tacchella et al.'s (2015) method of using the Sersic fit of galaxies, which they pointed out minimizes the effects of the PSF on the result. We use both the B and the R bandpass Sersic fits to then calculate the flux density within a 1 kpc aperture in each bandpass. These flux densities are then used to calculate the B-R color, with which we use to acquire $M/L_{\rm B}$ using the relation from Bell & de Jong (2001). The magnitude in the X band, where X can be the B band, the R band or any other band of interest, is calculated as

$$M_X = -2.5\log_{10}\left(\frac{f_X}{f_{0,X}}\right) \qquad (3)$$

where $f_{0,X}$ is the zero point flux density, in Jy, for band X, which we acquire from the SVO Filter Profile Service, and f_X is the flux density of the Sersic fit within the 1 kpc aperture. In order to calculate f_X, we have to convert the output of SKIRT which is in units of W/m^{2}arcsec^2 to Jy. The calculation is as follows:

$$f_X = 1000A\frac{\lambda_{eff,X}}{c}\sum_{i,j<1\mathrm{kpc}} I_{ij} \quad (4)$$

where $\sum_{i,j<1\mathrm{kpc}} I_{ij}$ is summing the surface brightness value of each pixel in the 1 kpc aperture, A is the area of the 1 kpc aperture in square arcseconds, 1000 is a conversion factor between W/m^2 and ergs/cm^2, and $\lambda_{eff,X}/c$, the effective wavelength divided by the speed of light, divides the quantity by the frequency which corresponds to λ_{eff} of the band X. These calculations are done for the B and the R bands and the B-R color is acquired as B-R=$M_B - M_R$, which is then fed into equation 2 to get M/L_B.

We additionally calculate B-R, and M/L_B, for an aperture corresponding to the Sersic fitted R_{80}, the radius which contains 80% of the galaxy's light. Thus, we get two different M/L_B ratios, one averaging over the inner 1 kpc of the galaxy, $(M/L_\mathrm{B})_{1\mathrm{kpc}}$, and the other averaging over the color out to R_{80}, $(M/L_\mathrm{B})_{\mathrm{R80}}$. We use these two values to discern the characteristics of the inner kpc with respect to the galaxy as a whole.

We calculate the stellar mass surface densities within 1 kpc and R_e, Σ_1 and Σ_e, *that an observer would infer from the synthetic images* by multiplying the 1 kpc and R_e light surface densities, measured in the B-band image, with the values of M/L_B. For each galaxy, we average Σ_1 and Σ_e over the different inclinations and acquire the error in the mean value by calculating the standard deviation of the values at each inclination. All errors reported in this paper at 1σ.

Some galaxy inclinations in our study were poorly fit with Sersic profiles, leaving large residuals when compared to the original unconvolved SKIRT image. As a result, we have excluded those inclinations with poor fits from the calculations of the aforementioned averages and standard deviations.

To compare the values inferred from the synthetic images with the intrinsic stellar surface density, we calculate the stellar half mass radius directly from each galaxy. We calculate the total mass within a sphere with a radius of the stellar half mass radius, and then divide by the area of a circle with the same radius to get the intrinsic surface density of the galaxy which we denote as the "Galdata" points in the next section. We do the same for a radius of 1 kpc. Additionally, we calculate mass projections for an observer at the same inclinations that we tell SKIRT to place detectors. Using these mass map projections, we calculate mass surface densities for a 1 kpc aperture and the 3D calculated stellar half mass radius. These points are labeled as the "Mass Map" points in subsequent plots.

In order to compare our mock observations to the size-mass relationship acquired by van der Wel et al. (2014), we produce mock observations of our galaxies at rest-frame 0.5 μm. We convolve the image with the aforementioned PSF and then fit the resulting convolved image with statmorph. The half light radius acquired this way provide a direct means of comparing the FIRE-2 galaxies to the relations derived by van der Wel et al. (2014) without including any observational effects of trying to calculate the M/L ratio. Since the galaxies that we analyze here are at z=1, which sits in between two of the redshift bins that van der Wel et al. (2014) use to acquire their size-mass relations, we choose to use their results calculated from the redshift bin with a midpoint of z=0.75. This relationship is given as

$$\log_{10}(R_\mathrm{e}/1\mathrm{kpc}) = (0.42 \pm 0.01) + (0.71 \pm 0.03)\log_{10}(M_\star/5\times10^{10}M_\odot) \quad (5)$$

for early type galaxies and

$$\log_{10}(R_\mathrm{e}/1\mathrm{kpc}) = (0.78 \pm 0.01) + (0.22 \pm 0.01)\log_{10}(M_\star/5\times10^{10}M_\odot) \quad (6)$$

for late type galaxies.

The size-mass, $\Sigma_1 - M_\star$ and $\Sigma_e - M_\star$ relations are different based on the galaxy being a star forming late type galaxy or a quiescent early type galaxy. As a result, we need to determine what the FIRE-2 halos considered here would be classified as. In order to do this, we follow the method of Williams et al. (2009) and use the rest-frame UVJ colors with the cutoff between early and late type galaxies being given by their equation 4. The band of interest here are the Bessell U and V bands (Bessell 1990), and the Mauna Kea definition for the J band (Tokunaga et al. 2002). To compute the color in a given band, we follow the procedure specified above for calculating the B and the R colors, except instead of using the Sersic fit to calculate the flux density in an aperture, we use the entire "original" unconvolved bandpass image to calculate the spatially integrated flux density.

3. RESULTS

An example of the procedure outlined in the prior section is shown in Figure 1, which shows the B band produced image from SKIRT, the B band image convolved with the PSF, the statmorph fitted Sersic 2D profile, and the residuals of subtracting the Sersic 2D fit from

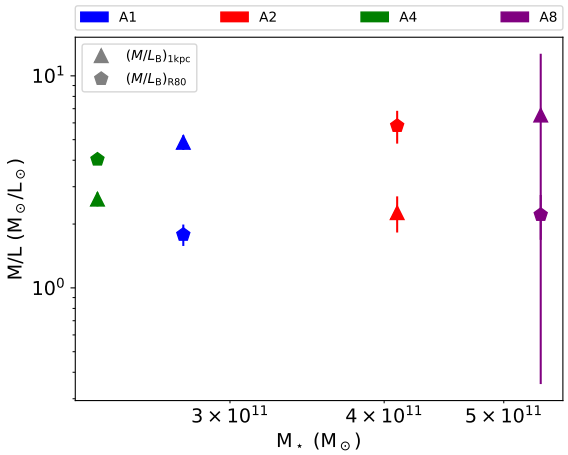

Figure 3. The calculated M/L_B ratio, averaged over the inner 1 kpc and R_e, for each galaxy.

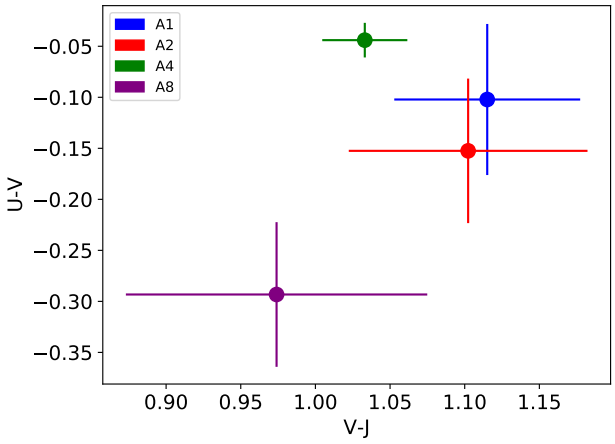

Figure 4. The distribution for the average restframe U-V color plotted against the V-J color. All of the FIRE-2 halos would be classified as star forming galaxies.

the unconvolved SKIRT image. Typically, the Sersic fits are able to account for $\gtrsim$90% of the light in the unconvolved SKIRT images.

Figure 2 shows the results of calculating the surface brightness profiles of the unconvolved B band image, the PSF convolved image, and the best fit Sersic profile to the galaxy, as shown in Figure 1. It is evident that the Sersic fit is able to reconstruct the profile of the unconvolved galaxy image.

As outlined in the previous section, we calculate the M/L_B ratio following the method outlined by Bell & de Jong (2001). In Figure 3 we plot the average values of $(M/L_B)_{1kpc}$ and $(M/L_B)_{R80}$ that are calculated for each galaxy. Galaxy A8 has relatively large error bars compared to the other galaxies due to the fact that 2 out of the 5 inclinations were poorly fit with a Sersic profile; thus, for this galaxy, we calculate averages over the remaining 3 inclinations, leading to relatively large 1σ deviations. The average M/L_B ratios that we acquire from all of the galaxies range between $\sim$2 - $\sim$5. The UVJ color for the FIRE-2 halos are also calculated and are plotted in Figure 4. Based on the criterion given by Williams et al. (2009), all of the halos would be classified as star forming.

Using the calculated M/L values (of each galaxy at every inclination) to convert our surface brightnesses, within a 1 kpc aperture and a half light radius aperture, to stellar mass surface densities, we can compare the mock observed surface densities of our galaxies to the empirical $\Sigma_1 - M_\star$ and $\Sigma_e - M_\star$ relations acquired by Barro et al. (2017). These results are shown in Figure 5, where the $\Sigma_1 - M_\star$ and $\Sigma_e - M_\star$ relations and the 1σ error in the scaling relations are shown. The average surface densities calculated directly from the FIRE-2 simulations and the projected stellar mass maps are plotted; they are approximately an order of magnitude greater than the observationally expected Σ_1 and approximately two orders of magnitude greater then the observationally expected Σ_e. The average stellar mass surface densities acquired from the mock observations are shown for the Sersic profile measured surface brightness densities multiplied by $(M/L_B)_{1kpc}$ and $(M/L_B)_{R80}$.

The mock observations for halos A2 and A4 are able to reproduce the observationally expected star forming values for the $\Sigma_1 - M_\star$ scaling relation when the $(M/L_B)_{1kpc}$ is used. When $(M/L_B)_{R80}$ is used, the Σ_1 values for these halos are larger by the same factor of $(M/L_B)_{R80}/(M/L_B)_{1kpc}$. Based on which M/L value is used, halo A1 is either over or under dense compared to the scaling relation. On the other hand, halo A8, on average, seems to be consistently under dense compared to the observationally expected value, even though the standard deviation between the different inclination angles is large. All of the galaxies, except for A8, are over dense compared to the $\Sigma_e - M_\star$ relation by a factor of $\sim$10-100. On average, galaxy A8 seems to be the only one that is able to recover the observationally expected Σ_e.

The behavior seen in Figure 5(b) can be explained by comparing the fitted R_e, of the FIRE-2 mock observations at 0.5 μm, to the scaling relation measured by van der Wel et al. (2014). This comparison is shown in Figure 6, where the late and early type relations and their 1σ intervals are plotted against each halo's average R_e, the star markers, and intrinsic 3D calculated stellar half mass radii, the circle markers labeled "Galdata". The FIRE-2 galaxies have R_e smaller than what is observationally expected; halos A1, A2, and A4 have $R_e \approx$

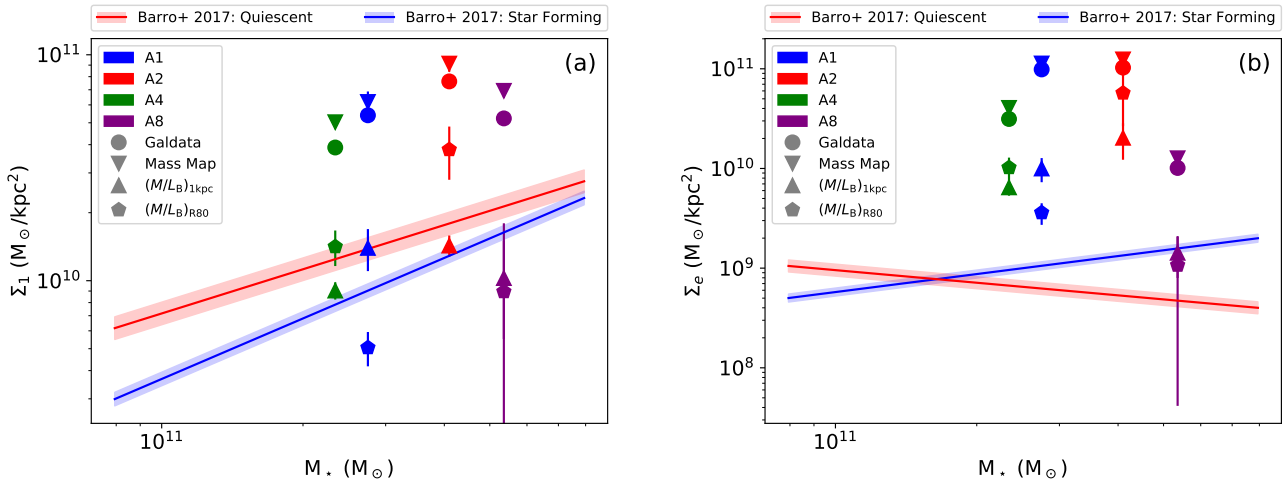

Figure 5. The calculated surface densities from the mock FIRE-2 images compared to the empirical scaling relations for $\Sigma_1 - M_\star$, shown in Figure (a), and $\Sigma_e - M_\star$, shown in the Figure (b). The "Galdata" and "Mass Map" points are calculated directly from the FIRE-2 simulations (see section 2) and the $(M/L_B)_{1kpc}$ and $(M/L_B)_{R80}$ points denote which M/L_B ratios were used to convert the light surface densities into stellar mass surface densities. Halos A2 and A4 are in agreement with the $\Sigma_1 - M_\star$ scaling relation, while A1 is either more or less dense than the relation based on the M/L ratio that is used. Halo A8 seems to be under dense than what Barro et al. (2017) find. All of the halos except for A8 are over dense compared to the $\Sigma_e - M_\star$ relation; halo A8 is able to reproduce the observationally expected Σ_e. In all cases, the observationally acquired stellar surface density values are lower than the true values calculated directly from the simulations.

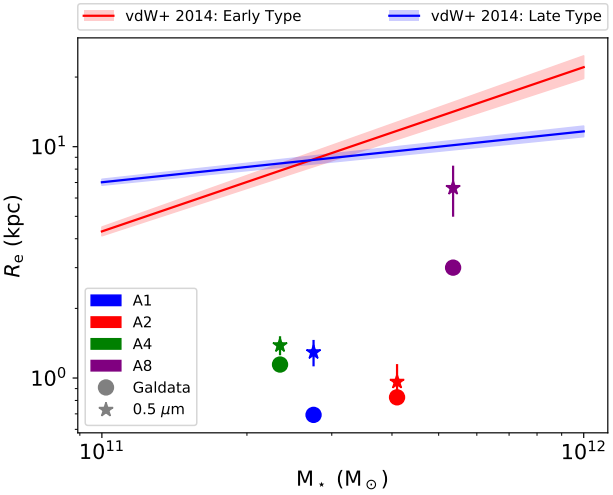

Figure 6. Plotted are the intrinsic 3D stellar half mass radii for each halo, labeled as the "Galdata" points, and the measured R_e from the 0.5 μm mock observation of each galaxy. The R_e obtained from fitting the 0.5 μm mock FIRE-2 observations with a Sersic profile are smaller than what is observationally expected from the size mass relation measured by van der Wel et al. (2014) and the Galdata points are even smaller than what is derived from the mock observation.

1 kpc while for halo A8 $R_e \approx 6$ kpc; the 3D calculated stellar half mass radii are even smaller. This explains the high Σ_e measurements of halos A1, A2, and A4. Since $R_e \approx 1$ kpc for these halos, the area with which the surface density is being calculated over is not increasing with respect to the area of the aperture corresponding to 1 kpc (see Equation 1); We would expect the area to increase, since the scaling relation from van der Wel et al. (2014) shows that $R_e > 1$ kpc. Thus, the Σ_e measurements are probing the same properties as the Σ_1 measurements and the measured FIRE-2 Σ_e are essentially the same as the synthetic Σ_1 values. On the other hand, halo A8 has an average R_e that is still slightly less than the size-mass relation, however it's able to recover the observationally expected Σ_e relatively well. This halo has undergone a recent merger, as Anglés-Alcázar et al. (2017b) pointed out, which causes halo A8 to be less compact than the other 3 halos and have more material further from the center of the galaxy, as is evident by the fact that A8's stellar half mass radius is a factor of $\gtrsim$2 larger than the other halos.

4. SUMMARY AND DISCUSSION

We have run SKIRT radiative transfer simulations of the same four halos presented by Anglés-Alcázar et al. (2017b). These halos, originally presented in Feldmann et al. (2017), have been resimulated using the FIRE-2 code with the addition of other important physics (e.g. BH accretion).

We produce mock observations from the SKIRT output, at various inclinations, to produce broadband B images, using bandpass transmission functions, which are then convolved with a PSF with a FWHM of 0.16" to simulate the effects of observing with the Hubble

Space Telescope. After, the statmorph code (Rodriguez-Gomez 2018) is used to fit the convolved images with a Sersic profile. This Sersic profile is able to sufficiently reconstruct the morphology of the galaxy in the unconvolved image, and as a result we use the fitted profile to calculate the surface brightness densities in the inner 1 kpc and half light radius. These surface brightness densities are then converted to stellar mass surface densities by multiplying the values with M/L ratios that are calculated from the B-R color (Bell & de Jong 2001) in a 1 kpc and R_{80} aperture. The stellar mass surface densities are then compared to the scaling relations acquired by Barro et al. (2017).

We also produce images of the galaxies at 0.5 μm which are fit with statmorph; this allows us to acquire the half light radius for each galaxy at each inclination. The FIRE-2 R_e are then compared to the size-mass relation measured by van der Wel et al. (2014).

We find that:

- The R_e obtained from fitting the 0.5 μm mock FIRE-2 observations with a Sersic profile are smaller than what is observationally expected from the size mass relation measured by van der Wel et al. (2014). This shows that the FIRE-2 galaxies are too compact.

- The mock observed Σ_1 values for some of the halos are able to recover the observationally expected value when $(M/L_{\rm B})_{\rm R80}$ is used; Other halos are either over or under dense with respect to observations.

- The calculated Σ_e values for 3 out of the 4 halos are over dense, due to the fact that the fitted R_e are ~ 1 kpc which means that the measured Σ_e is equivalent to Σ_1. The only case where this does not occur is in halo A8, which had recently undergone a merger event. We speculate that this merger effected the distribution of stars in halo A8, permitting there to be more stars further away from the central core of the galaxy which effectively pulls the measured R_e out to larger radii. The calculated Σ_e for halo A8, using it's larger R_e, shows that it is in general agreement with the $\Sigma_e - M_\star$ relation.

In the future, we plan on looking deeper into the mass to light ratios that we acquire and understanding how they relate to the intrinsic mass to light ratios of the simulations. Future simulations will include the effects of AGN feedback and we plan on following the same procedure outlined in this paper to analyze those simulations and deterime if those simulations are less compact and able to reproduce the $\Sigma_1 - M_\star$, $\Sigma_e - M_\star$, and $R_e - M_\star$ relations. This will allow us to begin to pinpoint how AGN may play a role in galaxy formation.

This research has made use of the SVO Filter Profile Service (http://svo2.cab.inta-csic.es/theory/fps/) supported from the Spanish MINECO through grant AyA2014-55216. This work was initiated as a project for the Kavli Summer Program in Astrophysics held at the Center for Computational Astrophysics of the Flatiron Institute in 2018. The program was co-funded by the Kavli Foundation and the Simons Foundation. We thank them for their generous support.

REFERENCES

Anglés-Alcázar, D., Faucher-Giguère, C.-A., Kereš, D., et al. 2017a, Monthly Notices of the Royal Astronomical Society, 470, 4698

Anglés-Alcázar, D., Faucher-Giguère, C.-A., Quataert, E., et al. 2017b, Monthly Notices of the Royal Astronomical Society: Letters, 472, L109

Barro, G., Faber, S. M., Koo, D. C., et al. 2017, The Astrophysical Journal, 840, 47

Bell, E. F., & de Jong, R. S. 2001, The Astrophysical Journal, 550, 212

Bessell, M. S. 1990, Publications of the Astronomical Society of the Pacific, 102, 1181

Camps, P., & Baes, M. 2015, Astronomy and Computing, 9, 20

El-Badry, K., Wetzel, A., Geha, M., et al. 2016, The Astrophysical Journal, 820, 131

Feldmann, R., Quataert, E., Hopkins, P. F., Faucher-Giguère, C.-A., & Kereš, D. 2017, Monthly Notices of the Royal Astronomical Society, 470, 1050

Gültekin, K., Richstone, D. O., Gebhardt, K., et al. 2009, The Astrophysical Journal, 698, 198

Hopkins, P. F. 2015, Monthly Notices of the Royal Astronomical Society, 450, 53

Hopkins, P. F., Kereš, D., Oñorbe, J., et al. 2014a, Monthly Notices of the Royal Astronomical Society, 445, 581

Hopkins, P. F., Kereš, D., Oñorbe, J., et al. 2014b, Monthly Notices of the Royal Astronomical Society, 445, 581

Hopkins, P. F., & Quataert, E. 2011, Monthly Notices of the Royal Astronomical Society, 415, 1027

Hopkins, P. F., Wetzel, A., Kereš, D., et al. 2018, Monthly Notices of the Royal Astronomical Society, 480, 800

Leitherer, C., Schaerer, D., Goldader, J. D., et al. 1999, The Astrophysical Journal Supplement Series, 123, 3

Ma, X., Hopkins, P. F., Faucher-Giguère, C.-A., et al. 2015, Monthly Notices of the Royal Astronomical Society, 456, 2140

Rodriguez-Gomez, V. 2018, vrodgom/statmorph: v0.3.1, , , doi:10.5281/zenodo.1291691

Sersic, J. L. 1968, Cordoba, Argentina: Observatorio Astronomico, 1968

Skelton, R. E., Whitaker, K. E., Momcheva, I. G., et al. 2014, The Astrophysical Journal Supplement Series, 214, 24

Tacchella, S., Lang, P., Carollo, C. M., et al. 2015, The Astrophysical Journal, 802, 101

Tokunaga, A. T., Simons, D., & Vacca, W. 2002, Publications of the Astronomical Society of the Pacific, 114, 180

van der Wel, A., Franx, M., van Dokkum, P. G., et al. 2014, The Astrophysical Journal, 788, 28

Weingartner, J. C., & Draine, B. T. 2001, The Astrophysical Journal, 548, 296

Williams, R. J., Quadri, R. F., Franx, M., van Dokkum, P., & Labbé, I. 2009, The Astrophysical Journal, 691, 1879

Wuyts, S., Cox, T. J., Hayward, C. C., et al. 2010, The Astrophysical Journal, 722, 1666